



HAL
open science

New local electrical diagnostic tool for dielectric barrier discharge (DBD)

Clémence Tyl, Stéphane Martin, Céline Combettes, Gilles Brillat, Vincent Bley, Antoine Belinger, Simon Dap, Ronny Brandenburg, Nicolas Naudé

► **To cite this version:**

Clémence Tyl, Stéphane Martin, Céline Combettes, Gilles Brillat, Vincent Bley, et al.. New local electrical diagnostic tool for dielectric barrier discharge (DBD). *Review of Scientific Instruments*, 2021, 92 (5), 10.1063/5.0045654 . hal-04777974

HAL Id: hal-04777974


<https://hal.science/hal-04777974v1>

Submitted on 12 Nov 2024

HAL is a multi-disciplinary open access archive for the deposit and dissemination of scientific research documents, whether they are published or not. The documents may come from teaching and research institutions in France or abroad, or from public or private research centers.

L'archive ouverte pluridisciplinaire **HAL**, est destinée au dépôt et à la diffusion de documents scientifiques de niveau recherche, publiés ou non, émanant des établissements d'enseignement et de recherche français ou étrangers, des laboratoires publics ou privés.

AUTHOR QUERY FORM

	<p>Journal: Rev. Sci. Instrum.</p> <p>Article Number: RSI21-AR-00402</p>	<p>Please provide your responses and any corrections by annotating this PDF and uploading it to AIP's eProof website as detailed in the Welcome email.</p>
---	---	--

Dear Author,

Below are the queries associated with your article. Please answer all of these queries before sending the proof back to AIP.

Article checklist: In order to ensure greater accuracy, please check the following and make all necessary corrections before returning your proof.

1. Is the title of your article accurate and spelled correctly?
2. Please check affiliations including spelling, completeness, and correct linking to authors.
3. Did you remember to include acknowledgment of funding, if required, and is it accurate?

Location in article	Query/Remark: click on the Q link to navigate to the appropriate spot in the proof. There, insert your comments as a PDF annotation.
Q1	Please check that the author names are in the proper order and spelled correctly. Also, please ensure that each author's given and surnames have been correctly identified (given names are highlighted in red and surnames appear in blue).
Q2	Please define SMB at first occurrence.
Q3	In the sentence beginning "The setup is..." please confirm that "previous section" refers to Sec. V A.
Q4	Please confirm the page number in Refs. 13, 16, and 21, as we have inserted the required information.
Q5	<p>We were unable to locate a digital object identifier (doi) for Ref. 18. Please verify and correct author names and journal details (journal title, volume number, page number, and year) as needed and provide the doi. If a doi is not available, no other information is needed from you. For additional information on doi's, please select this link: http://www.doi.org/.</p> <p>Please confirm ORCID's are accurate. If you wish to add an ORCID for any author that does not have one, you may do so now. For more information on ORCID, see https://orcid.org/.</p> <p style="margin-left: 20px;"> Clémence Tyl – Stéphane Martin – Céline Combettes – Gilles Brillat – Vincent Bley – Antoine Belinger – Simon Dap – Ronny Brandenburg – Nicolas Naudé – 0000-0002-8534-4114 </p> <p>Please check and confirm the Funder(s) and Grant Reference Number(s) provided with your submission: Agence Nationale de la Recherche, Award/Contract Number ANR-16-CE92-0021 Deutsche Forschungsgemeinschaft, Award/Contract Number 316877802</p> <p>Please add any additional funding sources not stated above.</p>

Thank you for your assistance.

New local electrical diagnostic tool for dielectric barrier discharge (DBD)

Cite as: Rev. Sci. Instrum. 92, 000000 (2021); doi: 10.1063/5.0045654

Submitted: 28 January 2021 • Accepted: 3 May 2021 •

Published Online: 9 99 9999



View Online



Export Citation



CrossMark

Clémence Tyl,¹ Stéphane Martin,¹ Céline Combettes,¹ Gilles Brillat,² Vincent Bley,¹ Antoine Belinger,¹ Simon Dap,¹ Ronny Brandenburg,^{3,4} and Nicolas Naudé^{2,a)} 

AFFILIATIONS

¹LAPLACE, Université de Toulouse, CNRS, INPT, UPS, 31062 Toulouse, France

²Service Commun d'Electronique, SCEL-UPS, 31062 Toulouse, France

³Leibniz Institute for Plasma Science and Technology (INP), 17489 Greifswald, Germany

⁴Institute of Physics, University of Rostock, 18059 Rostock, Germany

^{a)} Author to whom correspondence should be addressed: nicolas.naude@laplace.univ-tlse.fr

ABSTRACT

A new diagnostic tool to study dielectric barrier discharges (DBDs) at atmospheric pressure by local electrical measurements is introduced. The square ground electrode is divided into 64 square segments (3.44 mm side length) so as to measure the discharge currents and gas voltages with spatial resolutions, which allows a 2D mapping. The electrical measurement results are validated by a comparison with short exposure time photographs taken from the top view of the discharge cell. For this purpose, we changed the local discharge behavior by varying locally the gas gap and the barrier capacitance and also by using a gas flow. Then, in both situations, the breakdown voltage depends on the position, and the discharge current and gas voltage are different as well. The measurements performed for a planar DBD in nitrogen with admixed nitrous oxide gas show that even if the discharge operates in a diffuse regime, the discharge does not behave exactly homogeneously on the whole surface area. The resulting electrical parameters allow us to refine the understanding of planar DBDs. The discharge activity changes the gas composition and thus the level of preionization in the direction of the gas flow. This influences the local breakdown voltage and thus the discharge morphology and local power density on the surface. The use of this new electrical diagnostic tool will allow us to refine the analysis of the spatial development of the discharge. This work gives some clues to improve the spatial resolution of this tool in the future.

Published under license by AIP Publishing. <https://doi.org/10.1063/5.0045654>

I. INTRODUCTION

As they do not require expensive vacuum systems, non-equilibrium atmospheric pressure plasma processes based on dielectric barrier discharges (DBDs) are tremendously popular as they are proposed for many applications. DBDs can be used in many processes, such as thin-film coating, sterilization, treatment of gases, aerodynamic flow control, and lighting devices.^{1–8} Depending on the gas, electrical operation parameters, and discharge geometry, the plasma operates in the classical filamentary mode or in a homogeneous regime.^{6,9,10} Homogeneous regimes are promising for surface modification applications as it allows us to uniformly transfer the energy to the surface. Consequently, it is easier to get homogeneous and dense layer deposition with a homogeneous discharge than with a filamentary plasma.¹¹

Electrical measurements are a convenient way to characterize the discharge regime and to study the discharge behavior. However,

because of the dielectric presence, it is not possible to directly measure the electrical parameters of the discharge. Usually, the gas voltage, discharge current, charge transferred within the discharge, and discharge power are calculated from the measured quantities (e.g., total current or charge) under the usage of an electrical equivalent circuit.^{12–15} Among other parameters, the electrical equivalent circuit depends on the DBD geometry and dimensions. The key parameter for this approach is the determination of the discharge area, which is usually considered to be equal to the electrode surface as the discharge is homogeneous. However, even if the plasma seems to cover the electrodes uniformly, its electrical properties (e.g., current density, breakdown voltage, and duration of discharge) are not exactly the same at any time and at any point of the surface. Then, it is preferable to speak about the diffuse discharge rather than the homogeneous discharge. The spatial variation can be due to the gas flow circulation as observed in a homogeneous discharge ignited by Townsend breakdown in nitrogen.¹⁶

60 For example, in surface treatment applications, a gas flow is
61 usually injected from one side of the planar DBD arrangement. The
62 residence time of the gas increases as a function of the position from
63 the gas inlet to the gas outlet. Thus, the species densities are not the
64 same along the gas flow because of the kinetic processes and chemical
65 reactions in the discharge.^{16,17} The discharge current and the gas
66 voltage are not uniform along the spatial DBD dimensions. There-
67 fore, the determination of discharge currents and gas voltages from
68 the 0D electrical equivalent circuit of the DBD is often erroneous,
69 corresponding, in fact, to mean values. In the best case, the calcu-
70 lated values are spatially averaged but do not allow the interpretation
71 of localized plasma treatment.

72 The spatial inhomogeneity of the characteristics of the diffuse
73 DBD in nitrogen is particularly highlighted with the addition of oxidi-
74 zing gases.¹⁶ For example, in the case of a Townsend discharge
75 in N₂ with 30 ppm of NO, the discharge is visually different from
76 the gas inlet to the gas outlet; the color changes from violet to green
77 along the gas flow.¹⁶ Even if the discharge is a diffuse one (i.e., with-
78 out filaments appearing on the electrical measurements), its behav-
79 ior changes along the gas flow direction and, therefore, the electrical
80 characteristics are also varying in the same way.

81 In order to have a more accurate characterization of the dis-
82 charge behavior, a measurement of the local current density is
83 required. A first prototype, using a ground electrode divided into
84 eight identical strips along the gas flow direction and a commercial
85 data acquisition system was successfully used in a previous publi-
86 cation.¹⁶ This setup allowed us to correlate the discharge current
87 and light emissions from different species in time and space (posi-
88 tion along the gas flow). The results highlighted the occurrence of
89 a memory effect involving oxidizing species when an oxidizing gas
90 is added to nitrogen.¹⁶ The approach using a segmented electrode
91 was previously used by Akishev for DC discharges at low pressure
92 with 100 sections.¹⁸ However, there were no time-resolved current
93 measurements, and the aim was only to study and control discharge
94 constriction.

95 Our first prototype is sufficient if the discharge modification
96 occurs only in 1D. However, for more complex discharge morpholo-
97 gies, this setup is not reliable. Therefore, the aim of this work is to
98 develop a new system that enables a 2D mapping of the electrical
99 parameters of a planar DBD. This approach will pave the way to high
100 resolution electrical diagnostics for DBDs.

101 II. ELECTRICAL DIAGNOSTIC OF A DBD

102 Usually, DBDs are characterized by electrical measurements
103 based on the applied voltage on the electrodes $V_a(t)$ and the current
104 delivered by the power supply $I_m(t)$. The latter is often deduced from
105 voltage measurements on a shunt resistor R_m in series with the cell
106 discharge.¹⁵ As explained above, it is not possible to measure the gas
107 voltage and the discharge current directly. Usually, these quantities
108 are calculated from the measured signals by using an equivalent elec-
109 trical circuit. The chosen equivalent circuit model of the discharge
110 cell is represented in Fig. 1. The gas volume is represented by two
111 electrical components C_g and G_g . The gas before the breakdown is
112 modeled by the capacitor C_g . The variation of the gas conductiv-
113 ity after its breakdown is modeled by the variable conductance G_g ,
114 which is in parallel with the capacitance C_g . The current in the gas is

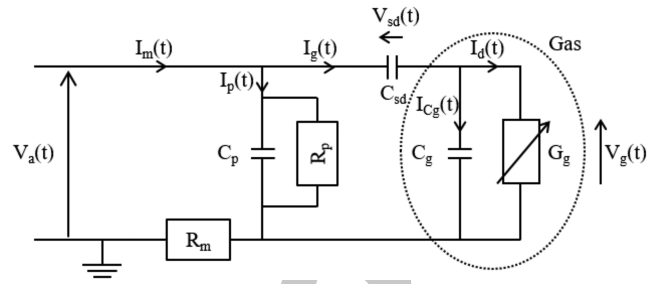


FIG. 1. Equivalent electrical circuit diagram of the discharge cell.

116 divided into two parts: the displacement current through the capac-
117 itance $I_{C_g}(t)$ and the discharge current $I_d(t)$. The measured current
118 $I_m(t)$ is the sum of the current through the gas $I_g(t)$ and a current I_p
119 originating from parasitic elements of the high voltage power sup-
120 ply system as well as the discharge cell. This part is represented by a
121 parallel circuit consisting of the resistor R_p and the capacitance C_p .
122 The values of these elements can be determined from $I_m(t)$ and $V_a(t)$
123 measured when the discharge is not (yet) ignited.

124 Before the discharge is ignited, the gas volume is purely capac-
125 itive with $G_g = 0$. Usually, the current I_m has a phase shift to the
126 voltage $V_a(t)$ slightly lower than 90°. This is due to the overall capac-
127 itive behavior of the discharge cell interfered by the parasitic resis-
128 tance R_p . The solid dielectrics are represented by the capacitance
129 C_{sd} in series with the elements representing the gas volume. In this
130 equivalent circuit, its value depends on the area of the electrodes,
131 the dielectric thickness, and the dielectric constant of the material.
132 Without discharge ($G_g = 0$), the discharge cell is equivalent to a RC
133 circuit with $R = R_p$, the equivalent resistance of the parasitic ele-
134 ments, and $C = C_{eq}$, the equivalent capacitance formed by C_p , C_g , and
135 C_{sd} [Eq. (1)]. The equivalent gas capacitance can be calculated from
136 the theoretical formula of a parallel-plate capacitor. The dielectric
137 capacitance C_{sd} can be also calculated knowing the relative permit-
138 tivity of the material or measured experimentally with an impedance
139 analyzer. Knowing the values of C_g and C_{sd} , it is possible to deter-
140 mine the values of R_p and C_p from a measurement without discharge
141 (by measuring the impedance module and the phase shift).

142 The current flowing through the discharge cell $I_g(t)$ is deduced
143 from the measured current $I_m(t)$ and the parasitic current $I_p(t)$
144 [Eq. (2)], with $I_p(t)$ calculated with Eq. (3),

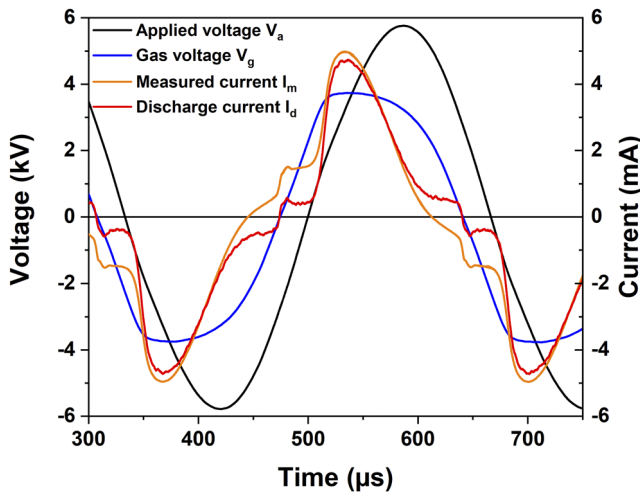
$$145 C_{equ} = \frac{C_{sd} \cdot C_g}{C_{sd} + C_g} + C_p, \quad (1)$$

$$146 I_g(t) = I_m(t) - I_p(t), \quad (2)$$

$$147 I_p(t) = \frac{V_a(t) - R_m I_m(t)}{R_p} + C_p \frac{d(V_a(t) - R_m I_m(t))}{dt}. \quad (3)$$

148 The applied voltage on the gas is deduced from Eq. (4), with $V_{sd}(t)$
149 calculated from Eq. (5). The constant $V_{sd}(t_0)$ is fixed such as the
150 $V_{sd}(t)$ mean value is equal to zero,

$$151 V_g(t) = V_a(t) - V_{sd}(t) - R_m I_m(t), \quad (4)$$



152 **FIG. 2.** Oscilloscope of a DBD in $N_2 + 25$ ppm O_2 , where gap = 1 mm, $f = 3$ kHz, $V_a = 11.5$ kV_{pp}, and $P_{surf} = 0.75$ W/cm².
153

$$V_{sd}(t) = \frac{1}{C_{sd}} \int_{t_0}^t I_g(\tau) d\tau + V_{sd}(t_0). \quad (5)$$

154
155 The discharge current $I_d(t)$ is deduced from Eq. (6), with $I_{Cg}(t)$ being
156 the part of the current due to the capacitive nature of the gas,

$$I_d(t) = I_g(t) - I_{Cg}(t) = I_g(t) - C_g \frac{dV_g(t)}{dt}. \quad (6)$$

158 The mean surface power density transmitted to the discharge is calculated for a given applied voltage frequency f from the gas voltage $V_g(t)$ and the discharge current $I_d(t)$ with Eq. (7) (S is the discharge area and T is the applied voltage period),
159
160
161

$$P_{surf} = \frac{f}{S} \int_0^T V_g(t) I_d(t) dt. \quad (7)$$

163 The evolutions of the discharge current $I_d(t)$, the gas voltage $V_g(t)$,
164 and the mean surface power density transmitted to the discharge
165 P_{surf} characterize the discharge and enable a better understanding
166 of the physical mechanisms. Figure 2 presents the gas voltage and

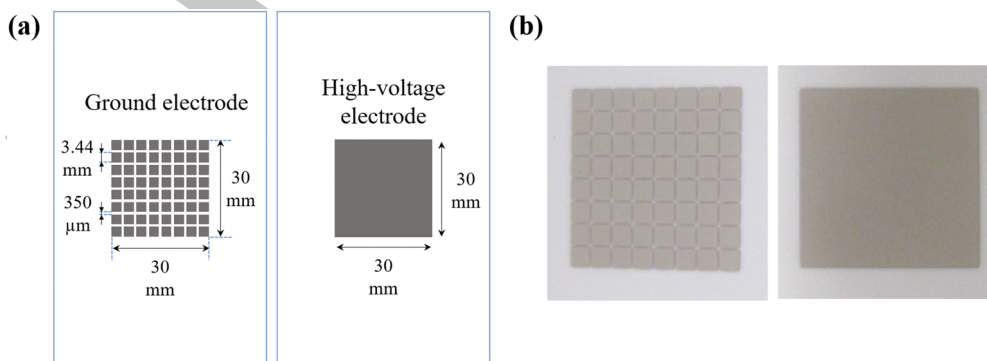
168 the discharge current calculated from the applied voltage and the
169 measured current (also shown) of a DBD in a mixture of nitrogen
170 with 25 ppm of oxygen with a gas gap of 1 mm. The electrode area is
171 $S = 9$ cm².

172 III. MANUFACTURING OF THE SEGMENTED 173 ELECTRODE

174 To get a 2D mapping of the discharge electrical parameters, the
175 ground electrode was prepared as a segmented electrode with 64
176 equally spaced square segments whereas the high voltage electrode
177 remained full. This electrode was a 3×3 cm² square, while each
178 square of the segmented electrode had a 3.44 mm side length with
179 a distance of 350 μ m as the gap between the segments (Fig. 3). The
180 electrode was realized by screen printing on alumina AD-96 from
181 CoorsTek (96% Al_2O_3) using a mix of silver and palladium (9916)
182 from Electro-Science Laboratories, Inc.

183 The electrical connections could not be made manually one by
184 one as the size of the segments was very small, and the number of
185 electrical wires would be difficult to handle. Instead, pins have been
186 brazed on each square segment and were connected to a printed circuit
187 board (PCB) to be able to plug in four connectors, each having
188 two rows of eight electrical contacts, as shown in Fig. 4(a). To ensure
189 the electrical insulation and avoid electric arcs, a silicone rubber
190 (Wacker[®] SEMICOSIL 915 HT, 1:1 mixed with Wacker[®] ELAS-
191 TOSIL CAT PT) has been poured around the pins as a layer of 2
192 mm thickness, resulting in a silicone gel layer after 30 min curing in
193 an oven at 100 °C, as shown in Fig. 4(b).

194 The discharge cell was placed in a gas vessel to ensure a controlled
195 atmosphere during the experiments. The experimental setup
196 has already been described in a previous publication.¹⁹ Two groups
197 of 32 wires connected the segmented electrode (with 4 connectors
198 with 16 wires each on the PCB) to the outside of the vessel through
199 two KF40 ports with two multi-pin vacuum connectors (Lesker
200 FTACIR32AS). On the outside of the vessel, two air-side circular
201 connectors (with 32 pins each) were plugged in the feedthroughs to
202 connect the segmented electrode to two housings with 32 resistors
203 of 3300 Ω each to be able to measure the current on each segment.
204 The two resistor housings have 32 SMB jacks each, which allowed
205 to measure the voltage at the terminals of the shunt resistors and
206 thus to deduce the current at each segment. First, a simple method
207 has been used to observe the different measured currents of the



167 **FIG. 3.** Diagram (a) and photograph (b) of the segmented electrode and the high voltage electrode. 208

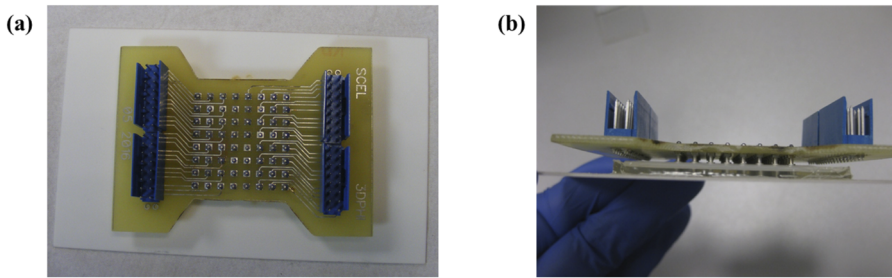


FIG. 4. PCB connected to the segmented electrode [(a) top view and (b) side view].

233
234

segmented electrode with an oscilloscope. The applied voltage was measured with a high voltage probe (P6015A from Tektronix) and recorded on channel 1 of an oscilloscope. A current transformer from Pearson Electronics (model 4100, 1 V/1 A ratio) was wrapped around the 64 wires outside of the reactor to measure and record the total current on channel 2 of the same oscilloscope. Furthermore, a dedicated data acquisition system, not described here, was developed to acquire the 64 currents but also the applied voltage and the total current (Fig. 5). Figure 6 shows the comparison between the current measured using the current probe with the sum of the currents measured for each segment of the segmented electrode. There is good agreement between the two currents demonstrating that the segmented electrode measurements cover the whole discharge activity.

IV. DETERMINATION OF THE CAPACITANCE VALUES OF THE SEGMENTED ELECTRODE

The data acquisition system allows us to acquire the applied voltage, the 64 local currents, and the total current (for comparison with the sum of the 64 currents to validate the measurements). As for a classical electrode configuration, it is not possible to acquire the gas voltages and the discharge currents for each zone (i.e., segment) directly. To calculate these values from the measured signals, the equivalent electrical circuit described above is used for each zone (Fig. 7). Each zone is considered as independent assuming

that no electric charges move from one zone to their neighbors. This assumption has been validated using a macroscopic electrical model of the discharge coupled with an electrostatic COMSOL[®] 2D model.²⁰ This simple model allows us also to compare the local discharge current in the gas gap with the discharge current calculated from the electrical measurements.

The segmented electrical model presented in Fig. 7 requires the knowledge about the values of the gas capacitance C_{gi} , the dielectric capacitance C_{sdi} , the parasitic resistance R_{pi} , and the parasitic capacitance C_{pi} for each segment labeled by subscript (Fig. 7). The calculation of the parasitic elements C_{pi} and R_{pi} applies the method described above to only one segment. Then, knowing the values of C_{gi} and C_{sdi} , it is possible to determine the values of C_{pi} and R_{pi} from the measurement of the current and the applied voltage when the discharge is turned off.

Hence, the main issue addressed with the segmented electrode is the determination of the values of C_g and C_{sd} and particularly of the effective surface of each segment. As the surface of each segment is relatively low (0.118 cm^2), a small error on the effective surface of each segment can change the precision of the results drastically. Moreover, due to the presence of the dielectric material, there is a spreading of the electric field lines. Because of edge effects, a different behavior can be expected between the inner segments and the segments that are located on the edges and the corners of the matrix as the spreading is not the same. To address this issue of surface determination, a COMSOL electrostatic 3D model of the segmented

235
236
237
238
239
240
241
242
243
244
245
246
247
248
249
250
251
252
253
254
255
256
257
258
259
260

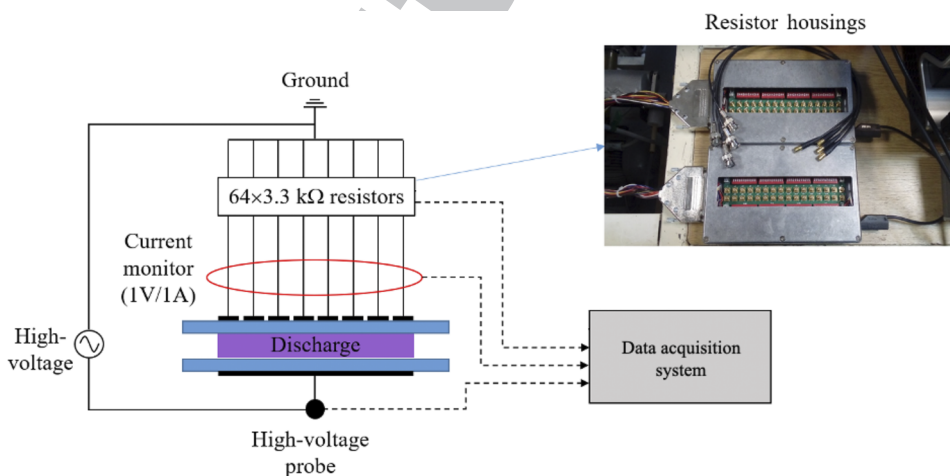


FIG. 5. Diagram of the connections of the segmented electrode for the electrical diagnostics.

261
262
263

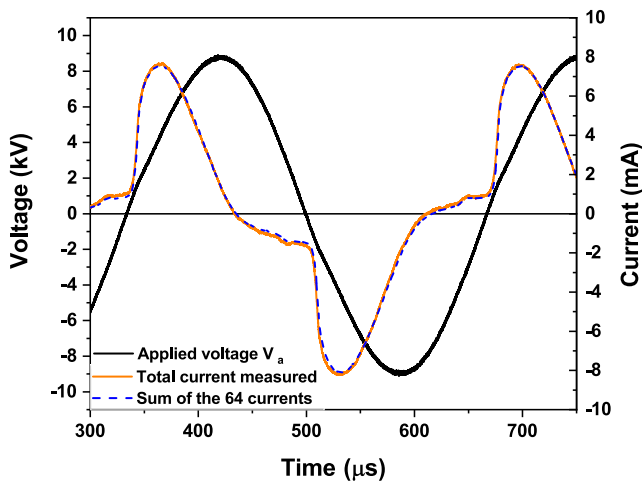


FIG. 6. Comparison between the total current measured using a current probe with the sum of the currents measured with the segmented electrode (N_2 , gap = 1 mm, $f = 3$ kHz, $V_a = 18$ kV_{pp}).

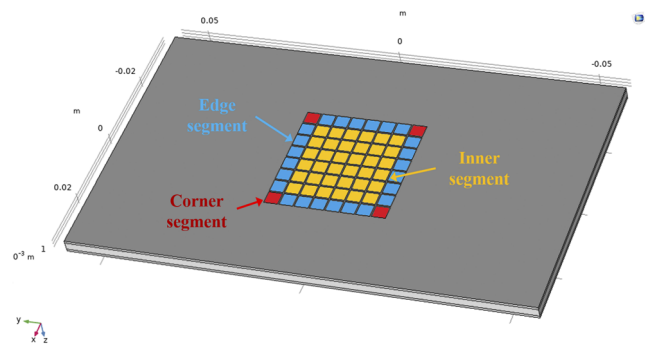


FIG. 8. COMSOL 3D model geometry of the discharge cell with the segmented electrode.

264
265
266

267
268
269
270
271
272
273
274
275
276
277
278
279
280
281
282
283
284
285

electrode (Fig. 8) was used to calculate the equivalent capacitance of the gas and the dielectrics. This model also allows us to confirm that the electric potential in the gas gap is not affected by the segmentation of the grounded electrode.

For a gas gap of 2 mm, Table I gives an example of the differences between the values obtained with COMSOL and theoretically. Two cases are considered for the theoretical calculations. First, the capacitances are calculated, with the surface areas of the segments being the same on all the positions and with a segment side of 3.44 mm. The sum of all the surfaces is 7.57 cm². It is equal to 84% of the surface of the non-segmented high voltage electrode (9 cm²). This means that the theoretical capacitances are underestimated. Hence, the capacitances are also calculated considering a surface of each segment equal to 9/64 = 0.1406 cm². Indeed, as the total current from the segmented electrode is the same as for the classical electrode configuration (Fig. 6), at least the same total surface should be considered.

The 3D electrostatic model of the cell discharge is also used to determine the equivalent capacitance of the gas and the dielectrics.

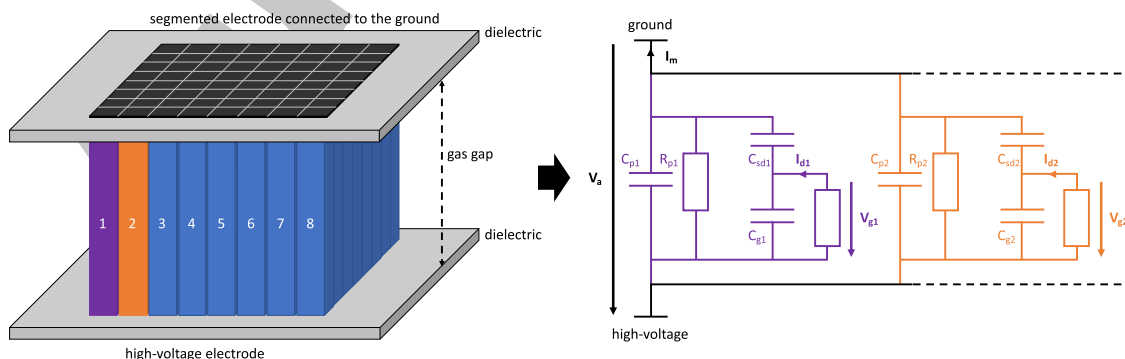


FIG. 7. Equivalent electrical circuit diagram of the discharge cell with the segmented electrode.

286

Then, another simulation determines the value of the dielectric capacitance C_{sd} by setting the gas gap to 0 mm. Then, the gas capacitance is deduced from these two values using the following equation:

$$C_{cell} = \frac{C_{sd} \cdot C_g}{C_{sd} + C_g}. \quad (8)$$

With the COMSOL calculation, the capacitance values C_{sd} for the edge and the corner are higher than the theoretical ones. For the capacitance values of the segment in the center of the segmented electrode, COMSOL calculation gives similar values than the theory. The sum of the calculated surfaces is equal to 9.34 cm², which is coherent with the surface deduced from the measurement with the impedance analyzer by using an alumina plate metallized ($S = 9$ cm²) on both sides and considering a relative permittivity equal to 9.6. Consequently, this method is chosen for the calculation of the electrical parameters with the segmented electrode as it is consistent with the calculation in the classical electrode configuration.

We can consider the outer segments as guard electrodes, ensuring a homogeneous electric field between the electrodes of the inner segments. The uncertainty on the surfaces and capacitances values is then more important for the corner and edge segments than for the inner segments.

287
288

289
290
291
292

293

294
295
296
297
298
299
300
301
302
303
304
305
306
307
308
309

310

TABLE I. Comparison of the theoretical and COMSOL values of the capacitances of the segmented electrode.

Calculation method	C_{cell} (pF)	S (cm ²)	C_g (pF)	C_{sd} (pF)	Total surface (cm ²)
Theory	$4.91 \cdot 10^{-2}$	0.1183	$5.24 \cdot 10^{-2}$	$7.92 \cdot 10^{-1}$	7.57
	$5.38 \cdot 10^{-2}$	0.1406	$6.22 \cdot 10^{-2}$	$9.41 \cdot 10^{-1}$	9
COMSOL	Center $5.96 \cdot 10^{-2}$	0.1424	$6.35 \cdot 10^{-2}$	$9.53 \cdot 10^{-1}$	9.34
	Edge $9.40 \cdot 10^{-2}$	0.1494	$1.03 \cdot 10^{-1}$	$9.99 \cdot 10^{-1}$	
	Corner $1.37 \cdot 10^{-2}$	0.1570	$1.58 \cdot 10^{-1}$	1.05	

V. VALIDATION OF THE MEASUREMENTS REALIZED USING THE SEGMENTED ELECTRODE

Before using the segmented electrode to study the physics of DBDs, it is necessary to validate it. To do that, the electrical diagnostics by the segmented electrode is combined with optical diagnostics, namely, iCCD camera imaging. Therefore, a DBD configuration with a transparent dielectric (quartz, thickness 1.1 mm) and a transparent electrode (indium tin oxide), connected to the high voltage, is used. The segmented electrode is connected to the ground, and an iCCD camera (PIMAX 3 Princeton Instruments) is placed vertically above the discharge cell to observe the spatial evolution of the discharge in two dimensions.

The studied discharge is always an atmospheric pressure townsend discharge (APTD)²¹ but without identical breakdown voltage and discharge current on all the electrode surfaces. In order to change the discharge morphology, we studied two conditions. First, the gas gap and the dielectric thickness is varied inside the discharge with a central glass wedge along the gas flow in order to locally change the discharge behavior by varying locally the gas gap and the barrier capacitance. Second, the segmented electrode is used to study a diffuse DBD in flowing gases with a constant gas gap, but due to the gas flow, the discharge behavior depends on the

gas residence time. In both situations, the breakdown voltage depends on the position, and the discharge current and gas voltage are different as well.

A. DBD with a central glass wedge along the gas flow

Two glass wedges with a 1 mm thickness (length 114 mm and width 19 mm) are placed between the dielectrics to set a gas gap of 1 mm. A glass wedge of $0.58 \times 114 \times 9.5 \text{ mm}^3$ is added in the middle between the 1 mm glass wedges, setting a gas gap of 0.42 mm for one third of the electrode area. The bottom dielectric on the central part is thicker as it is a stack of alumina and glass. Figure 9 shows the setup of the discharge cell in this configuration. This configuration has been tested in nitrogen N₂ (Alphagaz 2 from Air Liquide) with a gas flow rate of 500 SCCM and a frequency of 2 kHz. The measurements for two different voltages are presented thereafter at 11.5 and 14 kV_{pp}.

With an applied voltage of 11.5 kV_{pp}, the discharge is ignited at the central wedge position only, i.e., where the gas gap is smaller. Indeed, the currents measured by the segmented electrode show a clear difference between the segments located on the center under the central glass wedge and the other uncovered segments (Fig. 10). The discharge is ignited around 10 kV_{pp} on the center (gas gap of

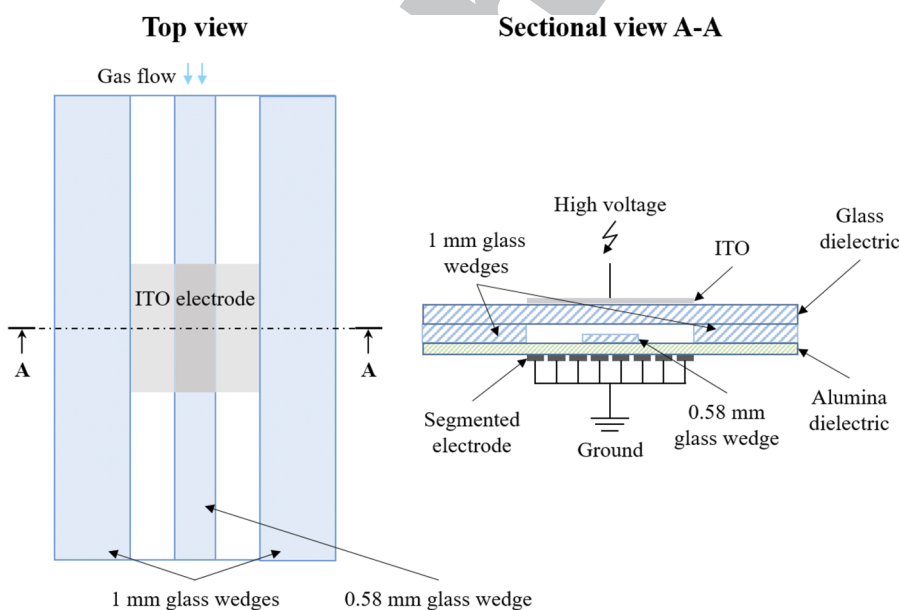


FIG. 9. Diagram of the discharge cell with a central glass wedge.

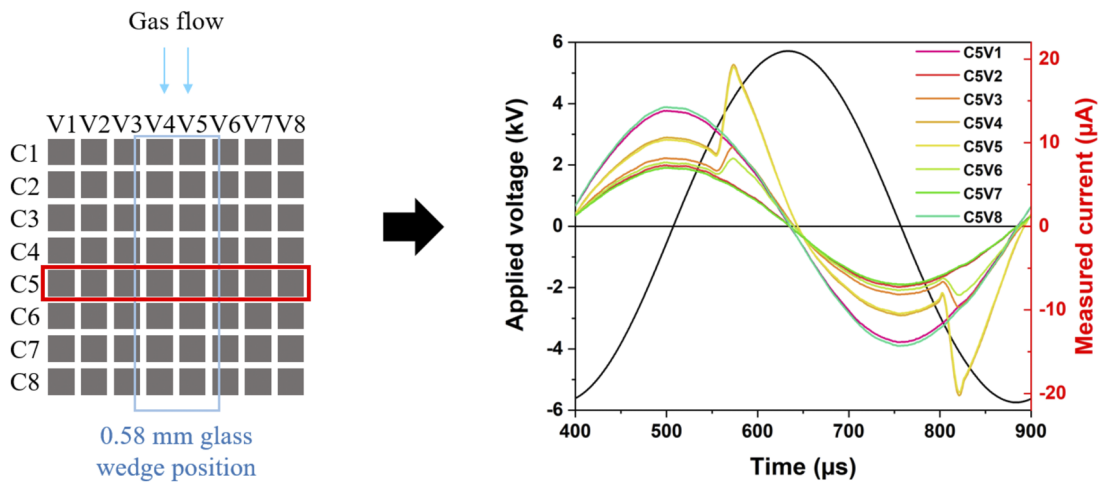


FIG. 10. Oscillogram of the local currents on the fifth line (N_2 , 500 SCCM, 2 kHz, 11.5 kV_{pp}).

366

383

0.42 mm) and at ~ 12 kV_{pp} on the two edges (gas gap of 1 mm). Thus, in this condition, the applied voltage is not sufficient to cause breakdown on the two edges. The discharge is ignited on the fourth and fifth segments along the gas flow (V4 and V5) and partially ignited on the third and sixth segments (V3 and V6) but not on the other ones. A photograph of the discharge with an exposure time equal to the duration of one period (500 μ s) in Fig. 11(a) clearly shows that the discharge is ignited in the central area only. The white dotted lines indicate the separation between the segments of the segmented electrode. The two lighter horizontal lines on the picture are due to CCD sensor damages. The photograph of the discharge correlates with a mapping of the surface power density shown in Fig. 11(b). The mean surface power density calculated with the total current is 0.032 W/cm², but its value is much higher on the central area, reaching 0.12 W/cm².

In the case of an applied voltage of 14 kV_{pp}, the discharge is ignited on the entire electrode cross section. However, the oscillogram of the total current in this case [Fig. 12(a)] shows that there are two current local maxima following each other. The oscillogram of the local currents on the fifth line in Fig. 12(b) shows that the discharge is first ignited on the third to sixth (and partially on the second and seventh) segments. Then, the discharge ignites on the other segments, while the current is already decreasing on the fourth and fifth segments.

The iCCD photograph of the discharge integrated over one period shows in this case that the discharge is ignited everywhere, but the light emitted by the discharge is stronger on the side areas where the gap is bigger [Fig. 13(a)]. As for the Fig. 11(a), the white dotted lines indicate the separation between the segments of the segmented electrode. The mapping of the surface power density

384
385
386
387
388
389
390
391
392
393
394
395
396
397
398

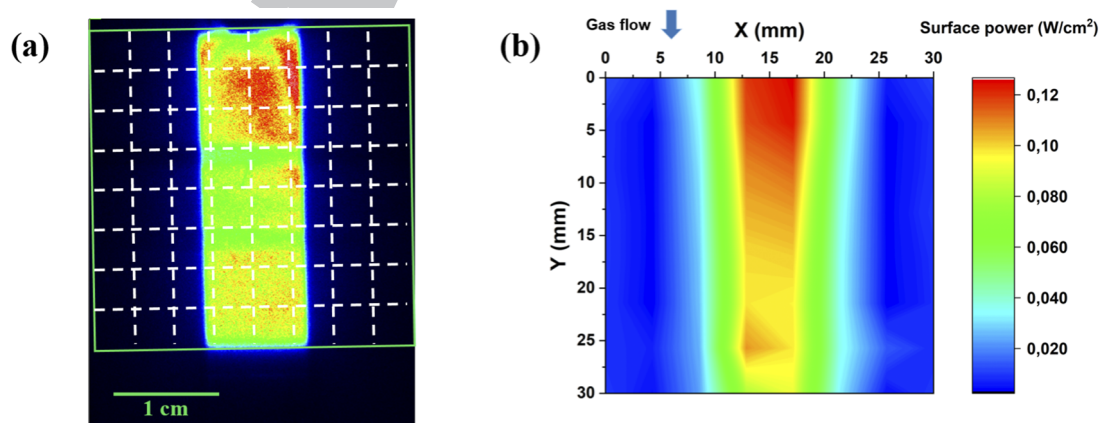


FIG. 11. (a) Photograph of the discharge with an exposure time of one period (500 μ s) and (b) mapping of the surface power density (N_2 , 500 SCCM, 2 kHz, 11.5 kV_{pp}).

382

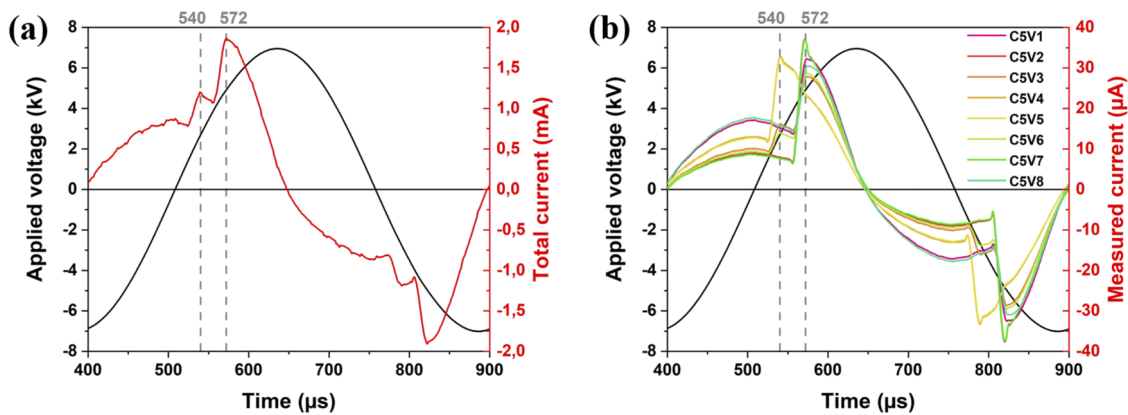


FIG. 12. Oscillograms of the measured total current (a) and local currents on the fifth line (b) with a central wedge (N_2 , 500 SCCM, 2 kHz, 14 kV_{pp}).

399

419

400 confirms this observation as the surface power density is higher on
401 the side areas. It varies from 0.17 to 0.29 W/cm² with an average
402 value of 0.21 W/cm². Note that even if the surface power density is
403 smaller in the center, the volume power density remains higher as
404 the gas gap is smaller.

405 In order to visualize the discharge ignition and evolution on
406 one period of the applied voltage, an acquisition with the iCCD
407 camera is also performed in sequential mode. A sequence of 250
408 images with a time exposure of 1 μs taken every 2 μs allows us to
409 follow the discharge emission over one full period (duration 500 μs).
410 Figures 14 and 15 compare photographs showing the discharge mor-
411 phology as well as maps of the measured current at two different
412 times: $t = 540 \mu s$ (coinciding with the first current local maxi-
413 mum; Fig. 14) and $t = 572 \mu s$ (corresponding with the second local maxi-
414 mum; Fig. 15). At $t = 540 \mu s$, the discharge is ignited on the central
415 zone only, whereas it is ignited everywhere at $t = 572 \mu s$. The mea-
416 sured current is maximum on the edge areas, whereas it decreases in
417 the center.

To conclude, in the center, as the gas gap is smaller, the gas
breakdown voltage is lower, which results in an earlier discharge
ignition at a lower momentary voltage. However, the local measured
current is smaller as the dielectric is thicker in this area, limiting the
current.

420

421

422

423

424

B. Spatial and temporal dynamics of a diffuse DBD in flowing gases

425

426

In this part, the segmented electrode is used to study a diffuse
DBD in N_2 and 30 ppm NO admixed with a total gas flow rate of 4
sLm and operated at a frequency of 2 kHz. The setup is similar to
Sec. V A (Fig. 9) but without the central glass wedge. The top glass
dielectric with the transparent electrode is replaced by an alumina
plate with a metal electrode in order to realize a fully symmetric DBD
arrangement (Fig. 3). It is measured that the electrical parameters of
the discharge are not the same along the gas flow direction. It is thus
necessary to analyze the local electrical parameters of the discharge.

427

428

429

430

431

432

433

434

435

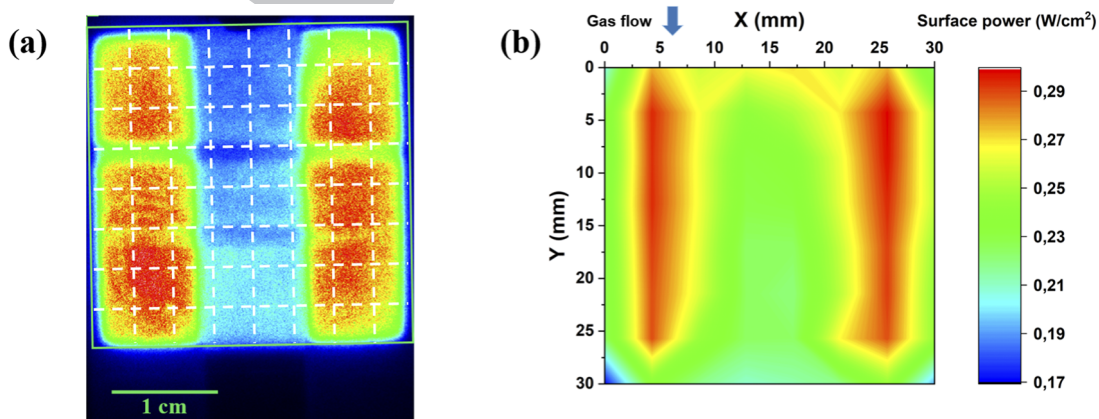
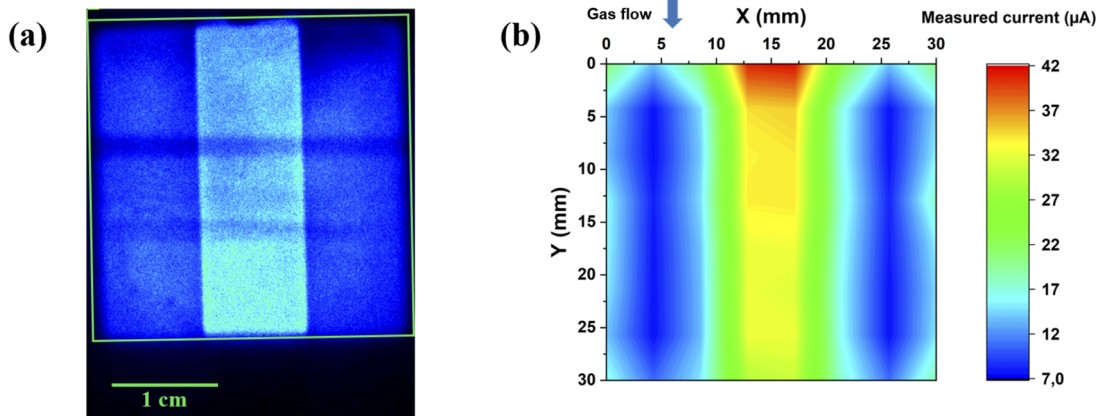


FIG. 13. (a) Photograph of the discharge with an exposure time of one period (500 μs) and (b) mapping of the surface power density (N_2 , 500 SCCM, 2 kHz, 14 kV_{pp}).

418

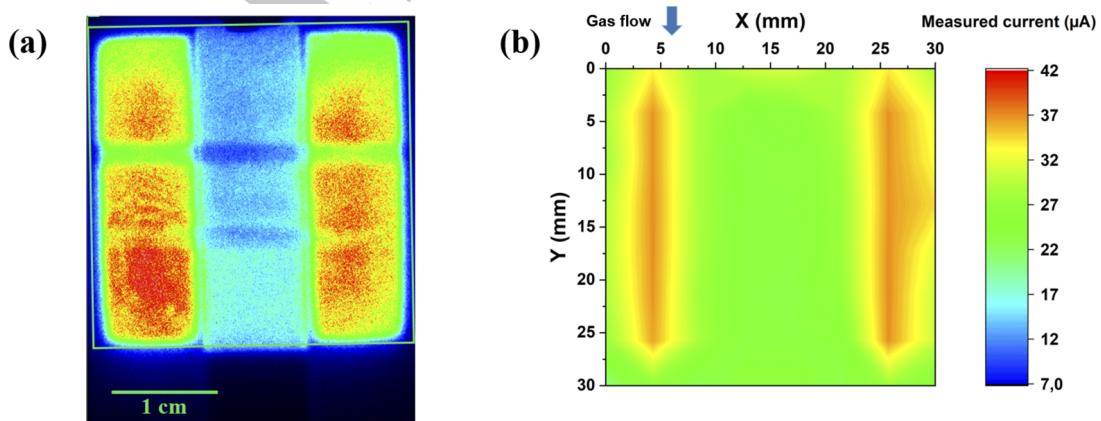


436 **FIG. 14.** (a) Photograph of the discharge with an exposure time of $1 \mu\text{s}$ and (b) mapping of the measured current at $t = 540 \mu\text{s}$, maximum of the first current peak (N_2 , 500
437 SCCM, 2 kHz, 14 kV_{pp}).

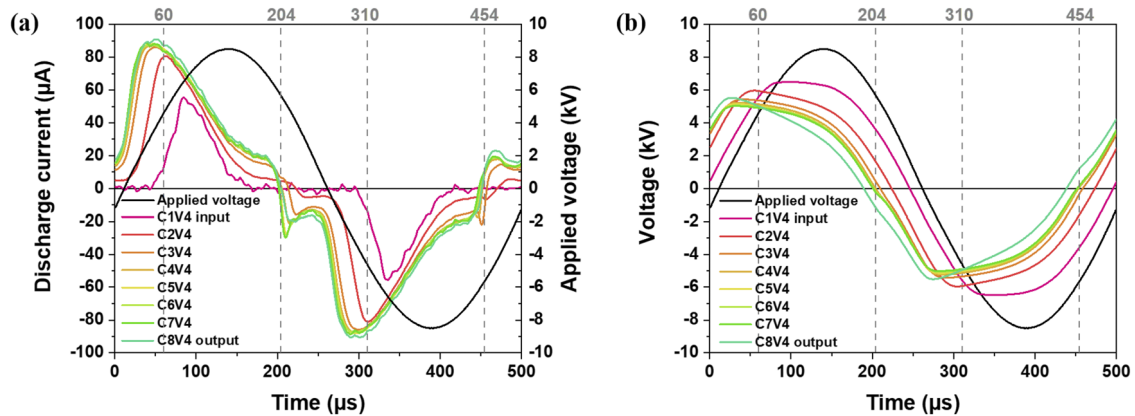
438 Figure 16 shows the temporal development of the discharge cur- 457
439 rents and the gas voltages calculated by the method described above 458
440 for different positions along the gas flow but for one of the central 459
441 columns (V4) of the electrode segments. It is clear from Fig. 16(a) 460
442 that the discharge is ignited at the output first and at the input 461
443 finally. The maximum of the discharge current is also higher at the 462
444 output. As the power density is lower at the input, there are less elec- 463
445 tric charges deposited on the dielectric surfaces, resulting in a lower 464
446 dielectric voltage V_{sd} . Therefore, the phase shift between the current 465
447 and gas voltage is also different from the input to the output, as can 466
448 be seen in Fig. 16(b). Therefore, the discharge not only is ignited later 467
449 at the input but is also turned off later. Once the discharge is ignited, 468
450 the gas voltage is almost constant, which is a property of an APTD.²¹ 469
451 When the applied voltage passes through its zero level, the discharge 470
452 is off but the current does not reach zero (see Fig. 2). This is linked 471
453 with a current jump, I_{jump} , when the gap voltage passes through 472
454 its zero level.¹⁶ The current jump, I_{jump} , manifests the memory 473

mechanism responsible for the production of seed electrons between 457
the voltage half periods and the two successive discharges. The 458
higher the current jump, the lower the breakdown voltage is and thus 459
the maximum the gas voltage. The decrease in the breakdown volt- 460
age with the gas residence time can be also partly due to an increase 461
in the gas temperature.²² 462

The calculated parameters from the total measured current are 463
 $P_{\text{surf}} = 1.10 \text{ W/cm}^2$, $I_{\text{jump}} = 79.6 \mu\text{A/cm}^2$, and $V_{g\text{max}} = 5.28 \text{ kV}$. 464
These values of the surface power density, the current jump, and 465
the maximum gas voltage can be compared with the local values as 466
a function of the position calculated with each measured segment 467
current, as presented in Fig. 17. The first result is the wide varia- 468
tion of these parameters from the gas input to the gas output. Along 469
the gas flow direction, the surface power density increases from the 470
input to around 10 mm reaching a plateau. The values vary from 0.4 471
to 1.3 W/cm^2 [Fig. 17(a)] in the first 10 mm. However, transverse to 472
the gas flow, the surface power density is nearly constant, except for 473



455 **FIG. 15.** (a) Photograph of the discharge with an exposure time of $1 \mu\text{s}$ and (b) mapping of the measured current at $t = 572 \mu\text{s}$, maximum of the second current peak (N_2 ,
456 500 SCCM, 2 kHz, 14 kV_{pp}).

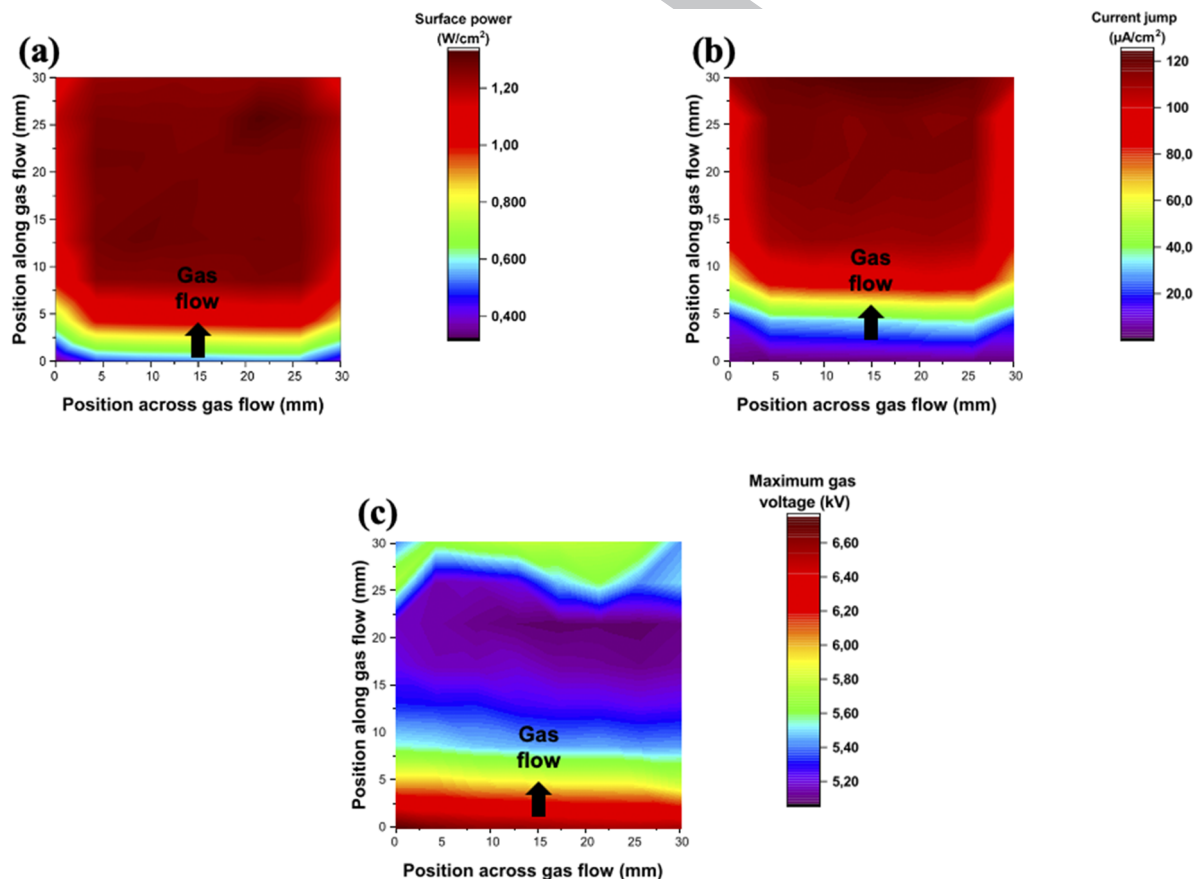


474 **FIG. 16.** (a) Discharge currents and (b) gas voltages on the fourth column of the segmented electrode along the gas flow in $N_2 + 30$ ppm NO (gap = 2 mm, 2 kHz, 17.12
475 kV_{pp}, 4 sLm).

476 the edge segments where the surface power density is lower, due to
477 the spreading of the discharge (see Sec. IV). The current jump has
478 the same behavior as the surface power density, namely, an increase
479 from the gas input to the gas output [Fig. 17(b)]. It also does not

vary much transversely to the gas flow, but it is slightly lower at the
edges. It also reaches a plateau at around 10 mm from the gas input.
The maximum gas voltage has an opposite development, being max-
imum at the gas input [Fig. 17(c)]. It decreases until around 23 mm

482
483
484
485



480 **FIG. 17.** 3D mapping of (a) surface power density, (b) current jump, and (c) maximum gas voltage resulting from measurements with the segmented electrode in $N_2 + 30$
481 ppm NO (gap = 2 mm, 2 kHz, 17.12 kV_{pp}, 4 sLm).

486 from the input and then slightly increases toward the output. The
487 latter is caused by the spreading of the discharge after the electrode
488 mainly due to the electric field and the blowing of active species by
489 the gas flow. The behavior of the maximum gas voltage shows that
490 the ignition voltage is higher at the gas input than at the gas output,
491 which is coherent with the current jump evolution. The higher the
492 memory effect, the lower the sustaining voltage.

493 It has been shown in the literature that the admixture of oxygen,
494 nitric oxide, or nitrous oxide changes the overall discharge in gen-
495 eral and the breakdown voltage in particular.^{16,23–25} Up to a gas type
496 dependent value in the range of some 100 ppm, higher the amount
497 of such gases, lower the breakdown voltage. Obviously, the discharge
498 activity changes the local gas composition, forming N_xO_y with oxy-
499 gen impurities and affecting the discharge behavior, morphology,
500 and local energy deposition on the surface.

501 C. Areas for improvement of the diagnostic tool

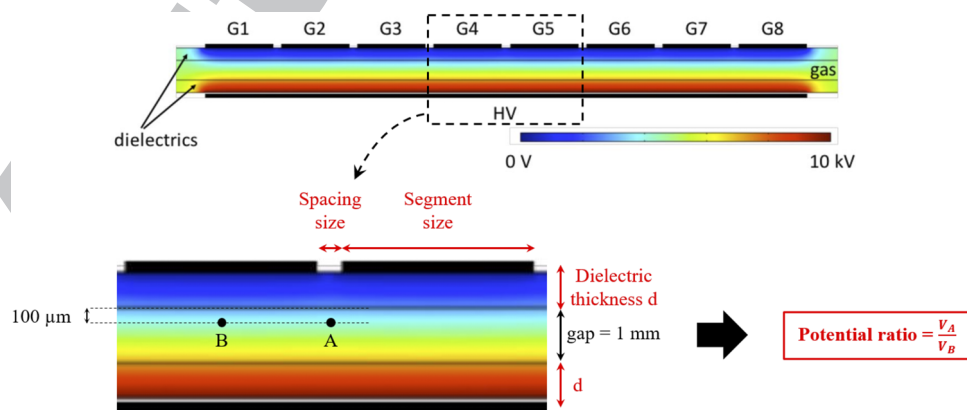
502 The previous examples on the investigation of diffuse, but non-
503 uniform DBDs, confirm the need for a spatially resolved electrical
504 characterization. The spatial variation of discharge parameters is not
505 accessible on the mean values of the electrical parameters. The correla-
506 tion with the spatial emission profiles shows the direct correlation
507 between the electronic excitation of species and the local measured
508 currents.

509 The resolution of the diagnostic tool, both temporal and spatio-
510 nal, is a key issue for further studies. The temporal resolution is
511 determined by the acquisition system. The system used here has
512 been designed by the electronic department of the LAPLACE labo-
513 ratory. Its sampling rate can be adjusted from 10 Hz to 10 MHz
514 with a memory depth of 4096 points for each signal. The spatial
515 resolution depends on the size and the number of the segments.
516 Concerning the acquisition system, the number of segments can be
517 increased and only requires an increase in the number of acquisition
518 boards. The main challenge is to reduce the size of the segments.
519 Indeed, the actual spatial resolution is not high enough to allow
520 an accurate investigation of self-organized DBDs with characteristic
521 discharge footprints of some 100 μm in diameter.²⁶ In the case of fil-
522 amentary DBDs, the filament radius is even smaller, typically around

524 100 μm .²⁷ Thus, the present size of the segments does not allow to
525 resolve the current of one filament. Decreasing the size of the seg-
526 ments would allow to broaden the scope of the types of discharges
527 to be studied with this new tool. However, the size of the segments
528 cannot be decreased without altering the overall behavior of the
529 discharge.

530 In order to explore the limitation of segment size reduction, a
531 2D electrostatic simulation has been carried out with COMSOL. It
532 allows us to study the influence of the thickness of the dielectrics,
533 the spacing between the segments, and the size of the segments on
534 the electric potential in the gas gap. In order to have a 2D model,
535 the geometry is the same as the configuration from the first seg-
536 mented electrode prototype,¹⁶ with a division of the ground electro-
537 de into eight strips $30 \times 3.4 \text{ mm}^2$, separated by 350 μm , a gas
538 gap of 1 mm, and two 635 μm thick dielectrics made of alumina
539 ($\epsilon_r = 9.6$). To quantify the influence of the division of the grounded
540 electrode on the discharge, the electric potential is plotted in the gas
541 gap at a distance of 100 μm from the dielectric surface at two dif-
542 ferent positions: between two segments and at the center of one seg-
543 ment (points A and B in Fig. 18). Figure 18 illustrates the potential
544 ratio that is calculated in the simulations with the variable paramet-
545 ers in red. The more the ratio between the two potentials is far from
546 1, the more the equipotential lines are distorted by the division of the
547 electrode.

548 If the ground electrode is not segmented, points A and B are
549 on the same equipotential line and the potential ratio equals 1% or
550 100%. Starting from the initial geometry, three different parameters
551 are varied separately: (i) the thickness of the dielectrics from 100 μm
552 to 2 mm, (ii) the spacing between the segments from 1 μm to 2 mm,
553 and (iii) the size of the segments from 0.1 to 5 mm. The evolu-
554 tion of the potential ratio for the different cases is presented in
555 Fig. 19. Decreasing the dielectric thickness has an impact on the
556 potential ratio. For a thickness lower than 250 μm , the potential
557 ratio decreases greatly below 95% [see Fig. 19(a)]. Concerning the
558 spacing between the segments, the potential ratio falls drastically
559 below 95% for distances above the thickness of the dielectric 650 μm
560 [Fig. 19(b)]. Those two parameters have a significant impact on the
561 potential ratio and thus on the discharge. However, their values in
562 the present arrangement show that the discharge is not impacted.



523 FIG. 18. Diagram of the potential ratio calculation in the COMSOL 2D electrostatic simulation.

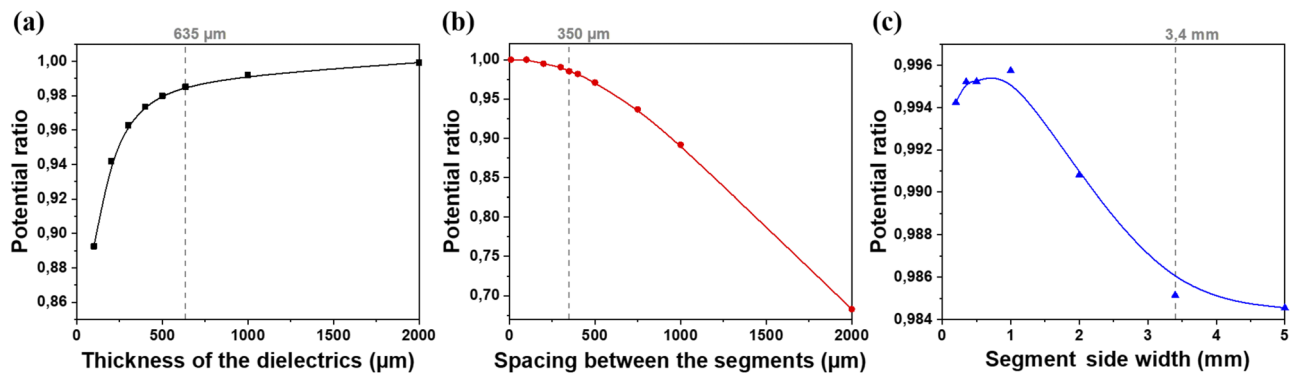


FIG. 19. Variation of the potential ratio as a function of: (a) the thickness of the dielectrics, (b) the spacing between the segments, and (c) the size of the segments.

564

604

565 More generally, when the thickness of the dielectric is large compared to the spacing between the segments, the potential distribution and the discharge behavior is not affected by the segmentation. 566 Moreover, the segment width has almost no effect on the potential ratio. For the range being considered, the potential ratio is above 98% [Fig. 19(c)]. This shows that an electrode with smaller segments, 567 keeping the same spacing between the segments and the same dielectric thickness, could be considered to increase the spatial resolution. 568 However, reducing the size of the segments would also bring technical issues on the manufacture of the electrode and electrical connection of the segments. Methods other than screen printing might 569 be necessary to deposit the segments. The connection with the electrical circuit would require smaller pins or another technology (such as those used in microelectronics).

579 VI. CONCLUSION

580 A new electrical diagnostic tool for the study of diffuse or patterned dielectric barrier discharges (DBDs) has been developed. The electrode arrangement and measuring systems allow a 2D mapping of the discharge electrical parameters (e.g., discharge current, power dissipated, and gas voltage) of Townsend and glow discharges or hybrid or patterned regimes. It has been validated successfully on planar DBDs by the comparison with short exposure time photographs taken using a camera from above the discharge cell. It has been used to characterize the diffuse discharge (APTD) and shows the effect of a gas flow on the local electrical behavior of the discharge. In the case of diffuse DBDs with sinusoidal voltages at frequencies from 1 to 20 kHz, the temporal and spatial resolutions are high enough to characterize the behavior of the discharge with sufficient spatial information. It is shown that the higher the memory effect, which is responsible for the diffuse regime, the lower the sustaining voltage. As the discharge activity changes the local gas composition by forming N_xO_y species with oxygen impurities, the breakdown voltage is reduced. The diagnostic tool would be very useful to study the correlation between gas flow dynamics, local surface power dissipation, and plasma chemistry in surface layer deposition applications of DBDs.

600 In order not to modify the behavior of the discharge, special attention must be paid to the design and dimensions of the segments, in particular the spacing between the segments and the dielectric

thickness. Then, the use of this tool will allow us to refine the analysis of the spatial development of the discharge. Finally, some clues are provided to improve the spatial resolution of this tool in the future.

ACKNOWLEDGMENTS

The authors would like to acknowledge financial support from the Agence Nationale de la Recherche (REDBIRD Project No. ANR-16-CE92-0021). The authors acknowledge the national platform 3DPHI for its involvement in the production of segmented electrodes and the associated connections and packaging.

DATA AVAILABILITY

The data that support the findings of this study are available from the corresponding author upon reasonable request.

REFERENCES

- 1 B. Eliasson and U. Kogelschatz, *Appl. Phys. B* **46**(4), 299–303 (1988).
- 2 A. Sobel, *IEEE Trans. Plasma Sci.* **19**(6), 1032–1047 (1991).
- 3 J. L. Linsley Hood, paper presented at the Gas Discharges and Their Applications (GD 80), Edinburgh, Scotland, 1980.
- 4 W. Siemens, *Ann. Phys. Chem.* **178**(9), 66–122 (1857).
- 5 S. Samukawa, M. Hori, S. Rauf, K. Tachibana, P. Bruggeman, G. Kroesen, J. C. Whitehead, A. B. Murphy, A. F. Gutsol, S. Starikovskaia, U. Kortshagen, J.-P. Boeuf, T. J. Sommerer, M. J. Kushner, U. Czarnetzki, and N. Mason, *J. Phys. D: Appl. Phys.* **45**(25), 253001 (2012).
- 6 U. Kogelschatz, *Plasma Chem. Plasma Process.* **23**(1), 1–46 (2003).
- 7 H.-E. Wagner, R. Brandenburg, K. V. Kozlov, A. Sonnenfeld, P. Michel, and J. F. Behnke, *Vacuum* **71**(3), 417–436 (2003).
- 8 G. Fridman, G. Friedman, A. Gutsol, A. B. Shekhter, V. N. Vasilets, and A. Fridman, *Plasma Processes Polym.* **5**(6), 503–533 (2008).
- 9 P. J. Bruggeman, F. Iza, and R. Brandenburg, *Plasma Sources Sci. Technol.* **26**(12), 123002 (2017).
- 10 R. Brandenburg, *Plasma Sources Sci. Technol.* **26**(5), 053001 (2017).
- 11 F. Massines, C. Sarra-Bournet, F. Fanelli, N. Naudé, and N. Gherardi, *Plasma Processes Polym.* **9**(11–12), 1041–1073 (2012).
- 12 S. H. Liu and M. Neiger, *J. Phys. D: Appl. Phys.* **36**(24), 3144–3150 (2003).
- 13 A. V. Pipa and R. Brandenburg, *Atoms* **7**(1), 14 (2019).
- 14 A. V. Pipa, J. Koskulics, R. Brandenburg, and T. Hoder, *Rev. Sci. Instrum.* **83**(11), 115112 (2012).

- 642 ¹⁵F. Peeters and T. Butterworth, in *Atmospheric Pressure Plasma: From Diagnostics to Applications*, edited by A. Nikiforov and Z. Q. Chen (IntechOpen Limited, London, UK, 2019). 655
- 643 656
- 644 657
- 645 ¹⁶C. Tyl, X. Lin, M. C. Bouzidi, S. Dap, H. Caquineau, P. Segur, N. Gherardi, and 658
- 646 N. Naude, *J. Phys. D: Appl. Phys.* **51**(35), 354001 (2018). 659
- 647 ¹⁷X. Lin, C. Tyl, N. Naudé, N. Gherardi, N. A. Popov, and S. Dap, *J. Phys. D: Appl. 660*
- 648 *Phys.* **53**(20), 205201 (2020). 661
- 649 ¹⁸Y.-S. Akishev, A. P. Napartovich, S. V. Pashkin, V. V. Ponomarenko, N. A. 662
- 650 Sokolov, and N. I. Trushkin, *Zh. Tekh. Fiz.* **53**(12), 2351–2357 (1983). 663
- 651 ¹⁹F. Massines, N. Gherardi, A. Fornelli, and S. Martin, *Surf. Coat. Technol.* 664
- 652 **200**(5-6), 1855–1861 (2005). 665
- 653 ²⁰O. Levasseur, J. Profili, R. K. Gangwar, N. Naudé, R. Clergereaux, N. Gherardi, 666
- 654 and L. Stafford, *Plasma Sources Sci. Technol.* **23**(5), 054006 (2014).
- ²¹F. Massines, N. Gherardi, N. Naude, and P. Segur, *Eur. Phys. J.: Appl. Phys.* **47**(2), 22805 (2009). 655
- ²²N. Naudé, J.-P. Cambronne, N. Gherardi, and F. Massines, *J. Phys. D: Appl. 656*
- Phys.* **38**(4), 530–538 (2005). 657
- ²³R. Brandenburg, V. A. Maiorov, Y. B. Golubovskii, H.-E. Wagner, J. Behnke, 658
- and J. F. Behnke, *J. Phys. D: Appl. Phys.* **38**(13), 2187–2197 (2005). 659
- ²⁴E. Es-sebbar, N. Gherardi, and F. Massines, *J. Phys. D: Appl. Phys.* **46**(1), 015202 660
- (2012). 661
- ²⁵H. Höft, M. Kettlitz, M. M. Becker, and R. Brandenburg, *J. Phys. D: Appl. Phys.* 662
- 53**(2), 025203 (2019). 663
- ²⁶T. Callegari, B. Bernecker, and J. P. Boeuf, *Plasma Sources Sci. Technol.* **23**(5), 664
- 054003 (2014). 665
- ²⁷U. Kogelschatz, B. Eliasson, and W. Egli, *J. Phys. IV* **7**(C4), 47–66 (1997). 666